

**Multiple-relaxation-time model for the correct thermohydrodynamic equations**

Lin Zheng, Baochang Shi, and Zhaoli Guo\*

*National Laboratory of Coal Combustion, Huazhong University of Science and Technology,  
Wuhan 430074, People's Republic of China*

(Received 27 December 2007; revised manuscript received 12 May 2008; published 12 August 2008)

A coupling lattice Boltzmann equation (LBE) model with multiple relaxation times is proposed for thermal flows with viscous heat dissipation and compression work. In this model the fixed Prandtl number and the viscous dissipation problems in the energy equation, which exist in most of the LBE models, are successfully overcome. The model is validated by simulating the two-dimensional Couette flow, thermal Poiseuille flow, and the natural convection flow in a square cavity. It is found that the numerical results agree well with the analytical solutions and/or other numerical results.

DOI: [10.1103/PhysRevE.78.026705](https://doi.org/10.1103/PhysRevE.78.026705)

PACS number(s): 47.11.-j, 44.05.+e

**I. INTRODUCTION**

The lattice Boltzmann equation (LBE) method has been considered as a powerful numerical tool for simulating complex athermal or isothermal fluid flows and associated transport phenomena [1,2]. LBE was first proposed as a numerical scheme by McNamara and Zanetti [3], which obtained a smoother macroscopic behavior than the lattice gas. Unlike conventional numerical schemes based on discretization of the macroscopic continuum equation, the LBE is based on the microscopic or mesoscopic kinetic equation. The main ideas for LBE can be manifested by two aspects: One is that it treats the fluid on a statistical level and the particle density distribution function is solved by a discrete Boltzmann equation; another is to construct a simplified kinetic model that can represent the essential physics of microscopic or mesoscopic processes so that the macroscopic averaged properties can obey the desired macroscopic equations.

Because of the advantages of the LBE and easy boundary treatment, LBE has been applied to thermal flows. To clearly understand the mechanism of the thermal flows, recently, three categories of thermal LBE models have been proposed, i.e., the multispeed (MS) approach, the double-distribution-function (DDF) approach, and the hybrid approach. The MS approach is a straightforward extension of the athermal LBE for isothermal flows [4–15], which obeys the Boltzmann equation; the DDF approach utilizes two different distribution functions, one for the velocity field and the other for the temperature or internal energy field [16–24]; the hybrid approach can be considered as another version of the DDF approach [25]. Nevertheless, the energy equation in the hybrid approach is solved by different numerical methods rather than by LBE.

However, the application of MS, DDF, and hybrid approaches for thermal flows still has many challenges. The fundamental problem with most of the MS models is the insufficient truncation in the equilibrium distribution function and the lack of isotropy in the lattice model [26,27]. Furthermore, the fixed Prandtl number exists in most of the MS models, although this problem has been overcome by some modified models. Nevertheless, in most of the existing

improved MS models (except for Ref. [28]), the viscous coefficient in the energy equation is not consistent with that in the momentum equation [29–31] as  $Pr \neq 1$ : The transport coefficient of the viscous term appearing in the energy equation is the thermal conductivity rather than the shear viscosity. On the other hand, although the DDF models have improved numerical stability and can overcome the fixed Prandtl number problem, the DDF based approaches rely on the convenient mathematical artifacts whose purpose is merely to recover the three conservation equations at the continuum level, and the viscous heat dissipation and compression work done by the pressure were ignored by most of the models except for those proposed in Refs. [18–20]. Furthermore, all of the existing DDF models are “decoupling” models, i.e., the momentum equation adopts an equation of state with a constant temperature. This decoupling between the energy and momentum equations may result in a large error when applied to problems where the temperatures have significant influences on the velocity field. In the hybrid approach, the energy equation is solved by other numerical methods and the flow simulation was not only decoupled from the energy equation, but also usually ignored the viscous dissipation term and compression work.

It should be pointed out that, to the authors' knowledge, the improved MS model in Ref. [28] has firstly removed the inconsistent viscous problem between the momentum equation and the energy equation. However, to obtain the correct thermohydrodynamic equations, the third-order moments—the eigenvector of the collision matrix, of which the corresponding eigenvalue is related to thermal conductivity—are not in the frame of the lattice but the moving fluid [28]. This local varying eigenvector may require the collision operator to be varied locally and may be the reason for its few applications. The detailed analysis of this model can be found in Ref. [28].

Up to date, most of the LBE models adopt the BGK collision model [32] which is approximated by a relaxation process with a single relaxation time. What should be mentioned is that the LBE models with multiple relaxation times (MRT) have also attracted much attention in recent years. Due to their apparent advantages over the BGK model [32], the MRT-LBE models have been successfully applied to a variety of isothermal flows [33–36] and recently formulated in a more general fashion [37].

Compared with the BGK model, the additional freedoms in the MRT model, i.e., different physical modes can be ma-

\*Corresponding author; [zlguo@hust.edu.cn](mailto:zlguo@hust.edu.cn)

nipulated independently in the moment space, provide a possible way to couple the momentum and temperature for thermal flows. The aim of this paper is to propose a coupling thermal MRT (TMRT) LBE model in the framework of single distribution function (SDF) in which the viscous dissipation and compression work are considered and the velocity and temperature fields are coupled.

The rest of the paper is organized as follows. In Sec. II, the TMRT model is proposed, and then a boundary condition for the model is introduced in Sec. III; some numerical tests are conducted in Sec. IV, and finally a brief summary is presented in Sec. V.

## II. THERMAL MULTIPLE-RELAXATION-TIME MODEL

A LBE with multiple relaxation times can be expressed as [34]

$$f_i(\mathbf{x} + \mathbf{c}_i \delta t, t + \delta t) - f_i(\mathbf{x}, t) = - \sum_{\alpha} S_{i\alpha} (f_{\alpha} - f_{\alpha}^{eq}) + \delta t \sum_{\alpha} \left( \delta_{i\alpha} - \frac{S_{i\alpha}}{2} \right) F_{\alpha}, \quad (1)$$

for  $i=0, 1, \dots, b-1$ , where  $f_i(\mathbf{x}, t)$  is the density distribution function for the molecules moving with a discrete velocity  $\mathbf{c}_i$  at point  $\mathbf{x}$  and time  $t$ ,  $\mathbf{S}$  is the collision matrix,  $\delta t$  is time step,  $f_i^{eq}$  is the equilibrium distribution function, and  $F_i$  is the forcing term given by [20,38]

$$F_i = \omega_i \rho \left( \frac{\mathbf{c}_i \cdot \mathbf{a}}{RT} + \frac{(\mathbf{c}_i \cdot \mathbf{u})(\mathbf{c}_i \cdot \mathbf{a})}{RT^2} - \frac{\mathbf{a} \cdot \mathbf{u}}{RT} \right),$$

where  $\mathbf{a}$  is the acceleration,  $\omega_i$  is the weight coefficient dependent on the model,  $R$  and  $T$  are the gas constant and temperature, respectively.

In LBE, the flow variables (density, momentum, and total energy) are defined as the velocity moments of distribution functions

$$\rho = \sum_i f_i, \quad (2)$$

$$\rho \mathbf{u} = \sum_i c_i f_i + \frac{\delta t}{2} \rho \mathbf{a}, \quad (3)$$

$$\rho E = \sum_i \frac{c_i^2}{2} f_i + \frac{\delta t}{2} \rho \mathbf{u} \cdot \mathbf{a}. \quad (4)$$

The evolution of the LBE (1) can be decomposed into two substeps. i.e., the collision process,

$$f_i^{\dagger} = f_i(\mathbf{x}, t) - \sum_{\alpha} S_{i\alpha} (f_{\alpha} - f_{\alpha}^{eq}) + \delta t \sum_{\alpha} \left( \delta_{i\alpha} - \frac{S_{i\alpha}}{2} \right) F_{\alpha}, \quad (5)$$

and the streaming process,

$$f_i(\mathbf{x} + \mathbf{c}_i \delta t, t + \delta t) = f_i^{\dagger}.$$

The collision substep is not easy to carry out in the velocity space because  $\mathbf{S}$  is usually a full matrix. As shown in Refs. [33,34], it becomes convenient when the collision pro-

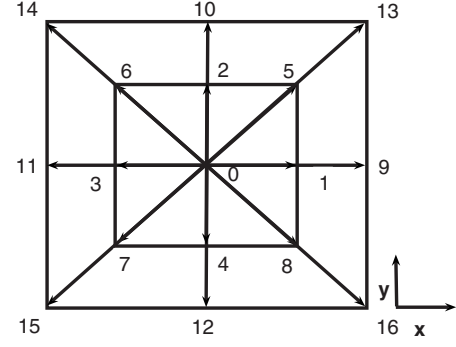


FIG. 1. Discrete velocities of D2Q17 model.

cess is carried out in the moment space. To this end, we first define some moments  $\mathbf{m}$  based on the distributions  $f(\mathbf{x}, t)$  through a linear transformation,

$$\mathbf{m} = \mathbf{M}f = [m_0, m_1, \dots, m_{b-1}]^T,$$

$$f = \mathbf{M}^{-1}\mathbf{m} = [f_0, f_1, \dots, f_{b-1}]^T,$$

where  $\mathbf{M}$  is a linear transformation which can be constructed from the discrete velocity set via the Gram-Schmidt orthogonalization procedure [25,33,34]. The conserved and nonconserved physical properties are clearly described in this process, including the density, the momentum, the kinetic energy, the energy flux, the viscous stress tensor, and so on. Therefore, by multiplying Eq. (5) by the linear transformation matrix  $\mathbf{M}$ , the collision in the moment space is now

$$m_i^{\dagger} = m_i - \sum_{\beta} \tilde{S}_{i\beta} (m_{\beta} - m_{\beta}^{eq}) + \delta t \sum_{\beta} \left( \delta_{i\beta} - \frac{\tilde{S}_{i\beta}}{2} \right) \tilde{F}_{\beta}, \quad (6)$$

where  $\mathbf{m}^{\dagger} = \mathbf{M}f^{\dagger}$ ,  $\mathbf{m}^{eq} = \mathbf{M}f^{eq}$  is the equilibrium in the moment space,  $\tilde{\mathbf{S}} = \mathbf{M}\mathbf{S}\mathbf{M}^{-1}$  is the corresponding collision matrix in the moment space and  $\tilde{F} = \mathbf{M}F$ .

It is noted that, to recover the Navier-Stokes-Fourier equations in the framework of SDF, the equilibrium of density distribution function should satisfy several conditions [4], or a lattice with sixth-order isotropy is required [5,6]. In this work we propose the following 17-velocity set (D2Q17) that fulfills these conditions for two-dimensional flows (see Fig. 1):

$$\mathbf{c}_i = \begin{cases} (0, 0), & i = 0, \\ \{\cos[(i-1)\pi/2], \sin[(i-1)\pi/2]\}c, & i = 1-4, \\ \{\cos[(2i-9)\pi/4], \sin[(2i-9)\pi/4]\}\sqrt{2}c, & i = 5-8, \\ \{\cos[(i-1)\pi/2], \sin[(i-1)\pi/2]\}2c, & i = 9-12, \\ \{\cos[(2i-9)\pi/4], \sin[(2i-9)\pi/4]\}2\sqrt{2}c, & i = 13-16, \end{cases} \quad (7)$$

where  $c = \delta x / \delta t = 1$ , with  $\delta x$  as the lattice space.

Based on these velocity vectors, we can construct a transformation matrix  $\mathbf{M}$  via the Gram-Schmidt process proposed by [25,33,34]

$$\mathbf{M} = \begin{pmatrix} 1 & 1 & 1 & 1 & 1 & 1 & 1 & 1 & 1 & 1 & 1 & 1 & 1 & 1 & 1 & 1 & 1 \\ 0 & 1 & 0 & -1 & 0 & 1 & -1 & -1 & 1 & 2 & 0 & -2 & 0 & 2 & -2 & -2 & 2 \\ 0 & 0 & 1 & 0 & -1 & 1 & 1 & -1 & -1 & 0 & 2 & 0 & -2 & 2 & 2 & -2 & -2 \\ -60 & -43 & -43 & -43 & -43 & -26 & -26 & -26 & -26 & 8 & 8 & 8 & 8 & 76 & 76 & 76 & 76 \\ 0 & 1 & -1 & 1 & -1 & 0 & 0 & 0 & 0 & 4 & -4 & 4 & -4 & 0 & 0 & 0 & 0 \\ 0 & 0 & 0 & 0 & 0 & 1 & -1 & 1 & -1 & 0 & 0 & 0 & 0 & 4 & -4 & 4 & -4 \\ 620 & 190 & 190 & 190 & 190 & -131 & -131 & -131 & -131 & -446 & -446 & -446 & -446 & 232 & 232 & 232 & 232 \\ -16 & 740 & 2248 & 2248 & 2248 & 7226 & 7226 & 7226 & 7226 & -6403 & -6403 & -6403 & -6403 & 1114 & 1114 & 1114 & 1114 \\ 84 & -64 & -64 & -64 & -64 & 56 & 56 & 56 & 56 & -14 & -14 & -14 & -14 & 1 & 1 & 1 & 1 \\ 0 & -4 & 4 & -4 & 4 & 0 & 0 & 0 & 0 & 1 & -1 & 1 & -1 & 0 & 0 & 0 & 0 \\ 0 & 0 & 0 & 0 & 0 & -4 & 4 & -4 & 4 & 0 & 0 & 0 & 0 & 1 & -1 & 1 & -1 \\ 0 & -14 & 0 & 14 & 0 & -11 & 11 & 11 & -11 & -10 & 0 & 10 & 0 & 14 & -14 & -14 & 14 \\ 0 & 4 & 0 & -4 & 0 & 1 & -1 & -1 & 1 & -5 & 0 & 5 & 0 & 1 & -1 & -1 & 1 \\ 0 & 32 & 0 & -32 & 0 & -28 & 28 & 28 & -28 & 14 & 0 & -14 & 0 & -1 & 1 & 1 & -1 \\ 0 & 0 & -14 & 0 & 14 & -11 & -11 & 11 & 11 & 0 & -10 & 0 & 10 & 14 & 14 & -14 & -14 \\ 0 & 0 & 4 & 0 & -4 & 1 & 1 & -1 & -1 & 0 & -5 & 0 & 5 & 1 & 1 & -1 & -1 \\ 0 & 0 & -32 & 0 & 32 & 28 & 28 & -28 & -28 & 0 & -14 & 0 & 14 & 1 & 1 & -1 & -1 \end{pmatrix}. \quad (8)$$

With this transformation matrix, we can obtain 17 velocity moments given by

$$\mathbf{m} = \mathbf{M}f \\ = [\rho, j_x, j_y, E', p_{xx}, p_{xy}, \varepsilon, h, H, \pi_{xx}, \pi_{xy}, q_x, \eta_x, \gamma_x, q_y, \eta_y, \gamma_y]^T,$$

which have clear physical significance:  $m_0$  is the mass density  $\rho$  (zeroth-order moment),  $m_1$  and  $m_2$  are the components of momentum,  $j_x$  and  $j_y$  (first-order moment),  $m_3 = E'$  is related to the total energy  $E$  (second-order moment). The rest moments are related to the stress tensor  $p_{xx}$  and  $p_{xy}$  (second-order moment), energy square  $\varepsilon$  (fourth-order moment), energy cubic  $h$  (sixth-order moment), energy quartic  $H$  (eighth-order moment), fourth-order moment  $\pi_{xx}$ , fourth-order moment  $\pi_{xy}$ ,  $x$  component of the energy flux  $q_x$  (third-order moment),  $x$  component of the fifth-order moment  $\eta_x$ ,  $x$  component of the seventh-order moment  $\gamma_x$ ,  $y$  component of the energy flux  $q_y$  (third-order moment),  $y$  component of the fifth-order moment  $\eta_y$ , and  $y$  component of the seventh-order moment  $\gamma_y$ , respectively.

As suggested in Ref. [34], the nonconserved moments relax linearly towards their equilibrium values that are functions of the conserved quantities. Therefore, for the D2Q17 model, the collision process (6) is operated by the following relaxation equations:

$$\mathbf{m}^+ = \mathbf{m} - \tilde{\mathbf{S}}(\mathbf{m} - \mathbf{m}^{eq}) + \delta t \left( \mathbf{I} - \frac{\tilde{\mathbf{S}}}{2} \right) \tilde{\mathbf{F}}, \quad (9)$$

where  $\tilde{\mathbf{S}}$  is the diagonal relaxation matrix in moment space,

$$\tilde{\mathbf{S}} = \text{diag}\{s_0, s_1, \dots, s_{16}\}, \quad (10)$$

and the equilibrium moments  $m_i^{eq}$  can be constructed accordingly as

$$\mathbf{m}^{eq} = [\rho, j_x, j_y, E', p_{xx}^{eq}, p_{xy}^{eq}, \varepsilon^{eq}, h^{eq}, H^{eq}, \pi_{xx}^{eq}, \pi_{xy}^{eq}, q_x^{eq}, \eta_x^{eq}, \gamma_x^{eq}, q_y^{eq}, \eta_y^{eq}, \gamma_y^{eq}]^T,$$

with  $s_i$  ( $i=0, 1, \dots, 16$ ) as the relaxation rate, and the corresponding equilibria of the conserved and nonconserved moments can be constructed as

$$m_0^{eq} = \rho, \quad (11)$$

$$m_1^{eq} = j_x = \rho u_x, \quad (12)$$

$$m_2^{eq} = j_y = \rho u_y, \quad (13)$$

$$m_3^{eq} = E' = \rho(\alpha + \beta E), \quad (14)$$

$$m_4^{eq} = p_{xx}^{(eq)} = \rho(u_x^2 - u_y^2), \quad (15)$$

$$m_5^{eq} = p_{xy}^{(eq)} = \rho u_x u_y, \quad (16)$$

$$m_6^{eq} = \varepsilon_{xx}^{(eq)} \\ = -\frac{109(30\rho + E'/2)}{3} - \frac{31E'}{3} + 436\rho\varepsilon(\varepsilon + \mathbf{u}^2) + \frac{109\rho\mathbf{u}^4}{2}, \quad (17)$$

$$m_7^{eq} = h^{(eq)} = 0, \quad (18)$$

$$m_8^{eq} = H^{(eq)} = 0, \quad (19)$$

$$m_9^{eq} = \pi_{xx}^{(eq)} = \left[ -\frac{65}{12} + \frac{17}{2} \left( \epsilon + \frac{\mathbf{u}^2}{6} \right) \right] p_{xx}^{(eq)}, \quad (20)$$

$$m_{10}^{eq} = \pi_{xy}^{(eq)} = \left[ -\frac{65}{12} + \frac{17}{4} \left( \epsilon + \frac{\mathbf{u}^2}{6} \right) \right] p_{xy}^{(eq)}, \quad (21)$$

$$m_{11,14}^{eq} = q_{x,y}^{(eq)} = [-17\rho + 6\rho(\epsilon + E)]u_{x,y}, \quad (22)$$

$$m_{12,15}^{eq} = \eta_{x,y}^{(eq)} = (c_1 + a_{x,y}\epsilon + b_{x,y}u_{x,y}^2)\rho u_{x,y} + c_{x,y}p_{xy}^{(eq)}u_{x,y}, \quad (23)$$

$$m_{13,16}^{eq} = \gamma_{x,y}^{(eq)} = (d_{x,y} + e_{x,y}\epsilon + f_{x,y}u_{x,y}^2)\rho u_{x,y} + g_{x,y}p_{xy}^{(eq)}u_{y,x}, \quad (24)$$

where  $\epsilon = RT$  is the internal energy. The parameters in the equilibrium are given as

$$\alpha = -60, \quad \beta = 34, \quad 4d_x - 62c_1 = -221, \quad d_x = -d_y,$$

$$a_x - \frac{2e_x}{31} = -\frac{249}{62}, \quad b_x - \frac{2f_x}{31} = -\frac{101}{62}, \quad c_x - \frac{2g_x}{31} = \frac{27}{31},$$

$$a_y + \frac{2e_y}{31} = -\frac{249}{62}, \quad b_y - \frac{2f_y}{31} = -\frac{101}{62}, \quad c_y + \frac{2g_y}{31} = \frac{27}{31}.$$

With the equilibria given by Eqs. (11)–(24), the thermo-hydrodynamic equations can be recovered from the LBE through the Chapman-Enskog expansion (see the Appendix for details),

$$\partial_t \rho + \nabla \cdot (\rho \mathbf{u}) = 0, \quad (25)$$

$$\partial_t (\rho \mathbf{u}) + \nabla \cdot (\rho \mathbf{u} \mathbf{u}) = -\nabla p + \nabla \cdot \boldsymbol{\tau}_1 + \rho \mathbf{a}, \quad (26)$$

$$\partial_t (\rho E) + \nabla \cdot [(p + \rho E) \mathbf{u}] = \nabla \cdot (\lambda \nabla T) + \nabla \cdot (\boldsymbol{\tau}_2 \cdot \mathbf{u}) + \rho \mathbf{u} \cdot \mathbf{a}, \quad (27)$$

where  $\boldsymbol{\tau}_1 = \mu[S - (\nabla \cdot \mathbf{u})\mathbf{I}]$ ,  $\boldsymbol{\tau}_2 = \frac{1}{2}\lambda[S - (\nabla \cdot \mathbf{u})\mathbf{I}]$  ( $S_{\alpha\beta} = \partial_\alpha u_\beta + \partial_\beta u_\alpha$ ), with

$$\mu = \rho \epsilon \left( \frac{1}{s_4} - \frac{1}{2} \right) \delta t, \quad (28)$$

$$\lambda = 2\rho \epsilon \left( \frac{1}{s_{11}} - \frac{1}{2} \right) \delta t, \quad (29)$$

$$p = \rho \epsilon, \quad (30)$$

It is obvious that this MRT LBE model can gain an arbitrary Prandtl number  $\text{Pr} = c_p \mu / \lambda$ , with  $c_p$  being the specific

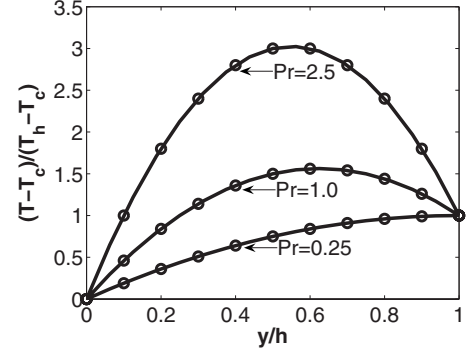


FIG. 2. Temperature profile of the Couette flow for  $\text{Ec}=8$ . Solid lines are analytic solutions and circles are numerical results.

heat ratio at constant pressure, by adjusting the relaxation rates  $s_4$  and  $s_{11}$ . However, it is noted that the viscous coefficient in the viscous dissipation term of the energy equation (27) is incorrect. Fortunately, with the benefit of using MRT, the collision process of each moment can be manipulated independently in the moment space. Motivated by the idea of Guo *et al.* [20], we propose to modify the collision process of the two moments related to the energy flux as

$$q_x^+ = q_x - s_{11}(q_x - q_x^{eq}) + \delta t(1 - s_{11}/2)\tilde{F}_{11} + (1 - s_{11}/2)q_x^*, \quad (31)$$

$$q_y^+ = q_y - s_{14}(q_y - q_y^{eq}) + \delta t(1 - s_{11}/2)\tilde{F}_{14} + (1 - s_{14}/2)q_y^*, \quad (32)$$

where  $q_x^*$  and  $q_y^*$  are given as

$$q_x^* = a_1 u_x p_{xx}^{(1)} + a_2 u_y p_{xy}^{(1)}, \quad (33)$$

$$q_y^* = b_1 u_x p_{xy}^{(1)} + b_2 u_y p_{xx}^{(1)}, \quad (34)$$

where  $a_1 = 3(\text{Pr} - 1)s_4$ ,  $a_2 = b_1 = 2a_1$ ,  $b_2 = -a_1$  and  $p_{\alpha\beta}^{(1)}$  is approximated as  $p_{\alpha\beta}^{(1)} \approx p_{\alpha\beta} - p_{\alpha\beta}^{(eq)}$ . With this modification, we are able to get the following correct thermohydrodynamic equations:

$$\partial_t \rho + \nabla \cdot (\rho \mathbf{u}) = 0,$$

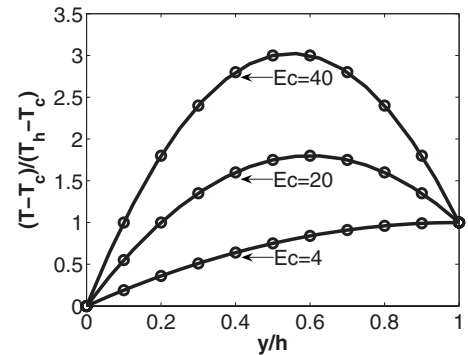


FIG. 3. Temperature profile of the Couette flow for  $\text{Pr}=0.5$ . Solid lines are the analytic solutions and circles are numerical results.

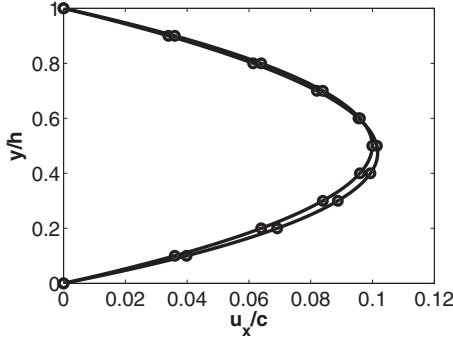


FIG. 4. Velocity profile of the thermal Poiseuille flow for  $Pr=0.71$ . Right to left:  $Ec=0.01, 50, 100,$  and  $150$ . Solid lines are the reference analytic solutions and circles are numerical results.

$$\partial_t(\rho\mathbf{u}) + \nabla \cdot (\rho\mathbf{u}\mathbf{u}) = -\nabla p + \nabla \cdot \boldsymbol{\tau}_1 + \rho\mathbf{a},$$

$$\partial_t(\rho E) + \nabla \cdot [(p + \rho E)\mathbf{u}] = \nabla \cdot (\lambda \nabla T) + \nabla \cdot (\boldsymbol{\tau}_1 \cdot \mathbf{u}) + \rho\mathbf{u} \cdot \mathbf{a},$$

### III. BOUNDARY CONDITION FOR TMRT MODEL

Boundary conditions for the lattice Boltzmann method have been studied extensively [39–41]. In order to transform a thermohydrodynamic boundary condition to the boundary distribution functions, we employ the nonequilibrium-extrapolation approach in this work due to its simplicity, second-order accuracy, and good robustness [42].

The basic idea of the nonequilibrium extrapolation can be interpreted as follows. At a boundary node  $x_b$  the distribution function can be decomposed into an equilibrium part and a nonequilibrium part, that is,

$$f_i(x_b, t) = f_i^{(eq)}(x_b, t) + f_i^{(neq)}(x_b, t).$$

For a boundary where  $\mathbf{u}(x_b, t)$  and  $E(x_b, t)$  at  $x_b$  are known, but  $\rho(x_b, t)$  is unknown, as an example, we use a temporary density  $\bar{\rho}(x_b, t)$  instead of the  $\rho(x_b, t)$  in the equilibrium distribution function

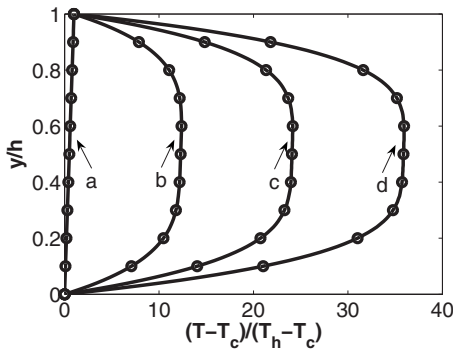


FIG. 5. Temperature profile of the thermal Poiseuille flow for  $Pr=0.71$ . (a)–(d)  $Ec=0.01, 50, 100,$  and  $150$ . Solid lines are the reference analytic solutions and circles are numerical results.

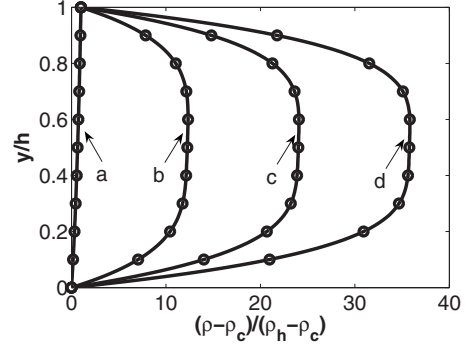


FIG. 6. Density profile of the thermal Poiseuille flow for  $Pr=0.71$ . (a)–(d)  $Ec=0.01, 50, 100,$  and  $150$ . Solid lines are the reference analytic solutions and circles are numerical results.

$$\bar{\rho}(x_b, t) = 3\rho(x_f, t) - 3\rho(x_{ff}, t) + \rho(x_{fff}, t),$$

where  $x_{ff}$  and  $x_{fff}$  are the nearest nodes in the vertical direction to the  $x_f$  and  $x_{ff}$ , respectively. As such, the equilibrium distribution function at  $x_b$  can be approximated as

$$f_i^{(eq)}(x_b, t) = f_i^{(eq)}[\bar{\rho}(x_b, t), \mathbf{u}(x_b, t), E(x_b, t)].$$

For the nonequilibrium part, we approximate it by the nonequilibrium part of the neighboring node  $x_f$ ,

$$f_i^{(neq)}(x_b, t) = f_i(x_f, t) - f_i^{(eq)}(x_f, t).$$

As a whole, the final distribution function at the boundary node  $x_b$  is given by

$$f_i(x_b, t) = f_i^{(eq)}(x_b, t) + [f_i(x_f, t) - f_i^{(eq)}(x_f, t)]. \quad (35)$$

It has been demonstrated that the nonequilibrium extrapolation scheme is of second-order accuracy in space [42].

### IV. NUMERICAL TESTS

In this section, we conduct a series of numerical simulations to validate the proposed TMRT LBE model. For simplicity, the parameters in the equilibrium are chosen as  $e_x = f_x = g_x = e_y = f_y = g_y = 0$  and others can be determined by their

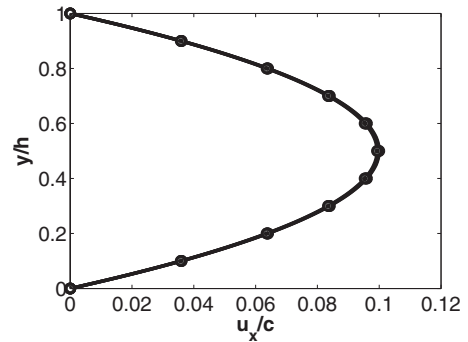


FIG. 7. Velocity profile of the thermal Poiseuille flow for  $Ec=50$ . Right to left:  $Pr=0.4$  and  $3$ . Solid lines are the reference analytic solutions and circles are numerical results.

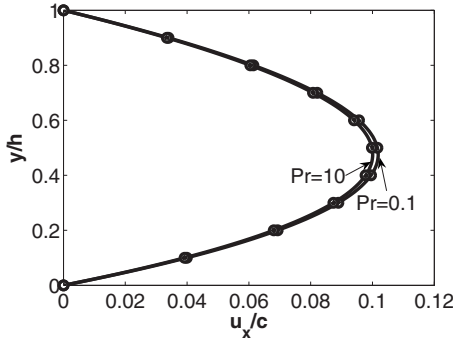


FIG. 8. Velocity profile of the thermal Poiseuille flow for  $Ec=0.01$ . Solid lines are the reference analytic solutions and circles are numerical results.

relations. The relaxation rates for conserved and nonconserved quantities, except for  $s_4$  and  $s_{11}$ , are given by 0 and 1.0, respectively. The testing problems include the Couette flow, Poiseuille flow, and the natural convection in a square cavity.

**A. Thermal Couette flow**

The Couette flow with a temperature gradient provides a good test of the ability of our TMRT model. With the bottom wall fixed and the top wall moving at speed  $U=0.1$ , the temperature profile can be described as

$$\frac{T - T_c}{T_h - T_c} = y^* + \frac{PrEc}{2} y^*(1 - y^*), \quad (36)$$

where  $T_c$  and  $T_h$  are the bottom and top wall's temperatures, respectively,  $y^*=y/h$  is the normalized distance from the bottom boundary, and  $h$  is the height of the channel.

The thermal Couette flow is characterized by the Prandtl number  $Pr$  and the Eckert number  $Ec=U^2/c_p(T_h-T_c)$ . In our simulations, we carried out the simulation on an  $8 \times 64$  lattice for different values of  $Pr$  and  $Ec$  with  $s_4^{-1}=1.1$  and  $T_c=0.6$ . Other parameters can be determined from the nondimensional parameters. Periodic boundary conditions are applied to the inlet and outlet, and the nonequilibrium-extrapolation method is applied to the top and bottom walls.

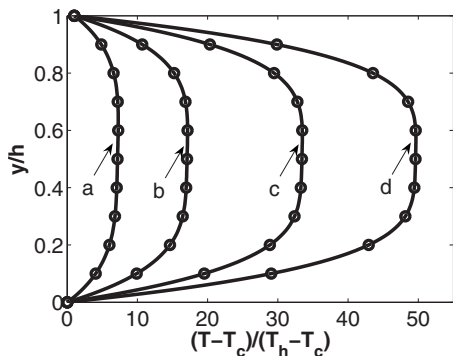


FIG. 9. Temperature profile of the thermal Poiseuille flow for  $Ec=50$ . (a)–(d)  $Pr=0.4, 1, 2,$  and  $3$ . Solid lines are the reference analytic solutions and circles are numerical results.

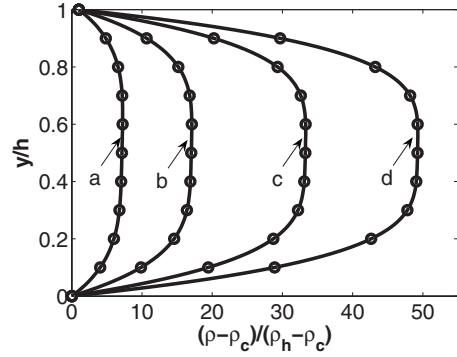


FIG. 10. Density profile of the thermal Poiseuille flow for  $Ec=50$ . (a)–(d)  $Pr=0.4, 1, 2,$  and  $3$ . Solid lines are the reference analytic solutions and circles are numerical results.

The temperature profiles for  $Ec=8$  with  $Pr$  varying from 0.25 to 2.5 are shown in Fig. 2, while the temperature profiles for  $Pr=0.5$  with  $Ec$  varying from 4 to 40 are shown in Fig. 3. It is clearly shown that the numerical results are in excellent agreement with the analytical solutions, and the viscous heat effects are successfully captured by the present TMRT model over a wide range of the values of  $Pr$  and  $Ec$ . Our numerical tests also indicate that the present LBE model is stable for the Couette flow as the temperature varies from 0.5 to 1.1, which is comparable to those of other MS models.

**B. Thermal Poiseuille flow**

The thermal Poiseuille flow in a planar channel considered here is driven by a constant force  $a$ , and the temperatures of the bottom and top walls are kept at  $T_c$  and  $T_h$ , respectively. In the thermal Poiseuille flow, the density  $\rho$  is not a constant but varies across the section since the momentum equation is coupled with the energy equation, and no analytic solutions for the velocity and temperature profiles are available. For comparisons, we first obtained numerical solutions of the thermohydrodynamic equations using a second-order finite-difference scheme as a reference.

The thermal Poiseuille flow is characterized by Reynolds number  $Re=\rho_r h u_r / \mu_r$ , Prandtl number, and Eckert number  $Ec=u_r^2/c_p(T_h-T_c)$ , with reference  $\rho_r$  and  $\mu_r$  measured at  $T_r=(T_h+T_c)/2$ ,  $u_r=\rho_r a h^2 / 8 \mu_r$ , and  $h$  being the channel height. We carried out a set of simulations for different values of  $Pr$

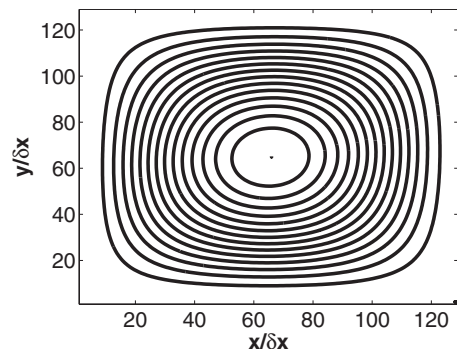


FIG. 11. Streamlines at  $Ra=10^3$ .

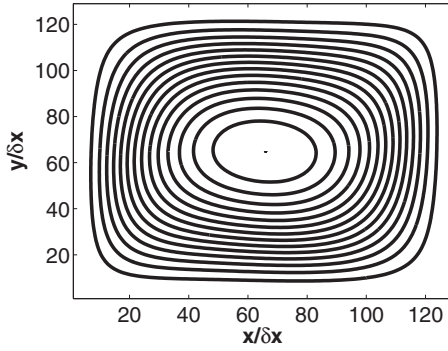


FIG. 12. Streamlines at  $Ra=10^4$ .

and  $Ec$  with  $Re=20$ ,  $T_c=0.6$ , and  $u_r=0.1$ . We first study the case when  $Pr=0.71$  with  $Ec$  ranging from 0.01 to 150. In our simulation, an  $8 \times 64$  lattice is employed, and other parameters are determined from the nondimensional parameters. The boundary treatment is the same as that used in the Couette flow. The velocity, temperature, and density profiles are shown in Figs. 4–6, respectively. It is clearly seen that temperature and density increase with  $Ec$ . However, due to the small temperature difference, except for  $Ec=0.01$ , the velocity profiles are almost overlapped when  $Ec=50, 100$ , and 150 (see Fig. 4).

We also conduct a series of simulations for  $Ec=50$  while  $Pr$  varies from 0.4 to 3. As can be seen from Fig. 7, the velocity profiles do not overlap as  $Pr=0.4$  and 3. To see more clearly this difference, we conduct the numerical test for  $Ec=0.01$  with  $Pr=0.1$  and  $Pr=10$ , and the velocity profiles are shown in Fig. 8. The reason for this phenomenon is attributed to the temperature-dependent viscous coefficient. The temperature profiles for different values of  $Pr$  are shown in Fig. 9, and the density profiles are shown in Fig. 10. It is clearly seen that the numerical results are in excellent agreement with the reference numerical solutions. It is again observed from Fig. 10 that the density profiles are not a constant but vary across the channel. This is due to the coupling between the velocity and energy fields, and thus such non-linear phenomena will not appear in a decoupling LBE model.

In the simulations, it is also observed that the  $y$ -direction component velocity,  $u_y$ , is nonzero ( $u_y/u_r \sim 10^{-4}$ ) as the temperature variation becomes large (e.g.,  $Ec=0.01$ ). This

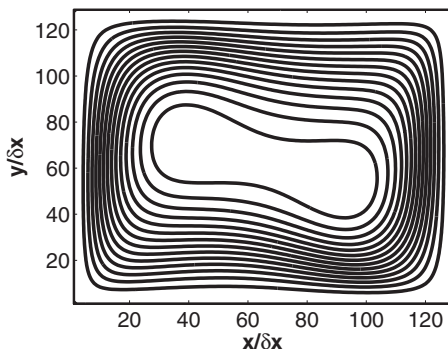


FIG. 13. Streamlines at  $Ra=10^5$ .

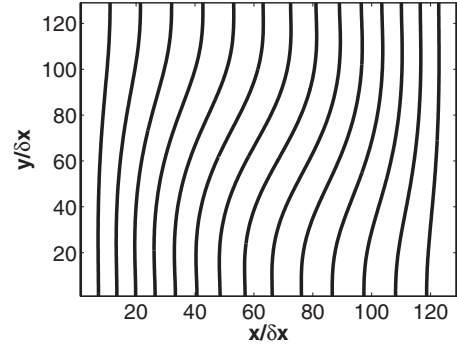


FIG. 14. Isothermal lines at  $Ra=10^3$ .

spurious velocity may be due to the boundary condition treatment for the unknown density distribution functions at the walls. It is noted that the similar phenomena was also observed by other LBE models in Ref. [43]. This unphysical artifact may be removed by using other more accurate schemes.

### C. Natural convection flow

The natural convection flow in a square cavity has been studied using the decoupling LBM [17,20,21]. In this problem, the two side walls are kept at temperatures  $T_h$  and  $T_c$ , respectively, with  $T_c < T_h$ , while the bottom and top walls are adiabatic. For the boundary conditions, the two side walls with constant temperatures are treated by the nonequilibrium-extrapolation method, but for the adiabatic boundary condition at the bottom or the top wall, the temperature at the boundary node  $x_b$  is first obtained by discretizing the macroscopic boundary condition,  $dT/dy=0$ , using a finite-difference scheme, and then we use this temperature in the nonequilibrium-extrapolation boundary condition. Such a treatment was also used in previous studies [17,20].

The convection flow induced by the temperature difference is characterized by the Prandtl  $Pr$  and the Rayleigh number,

$$Ra = \frac{gH^3(T_h - T_c)}{T_c \nu_c \alpha_c},$$

where  $\nu_c$  and  $\alpha_c$  are the values of the transport coefficients

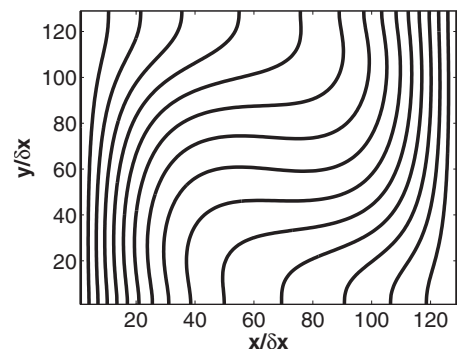
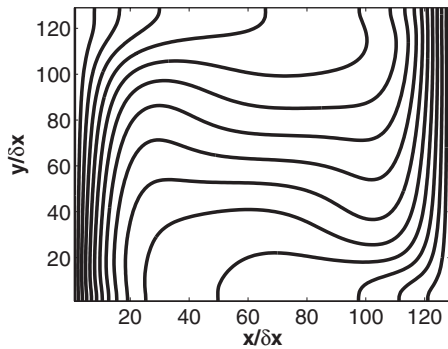


FIG. 15. Isothermal lines at  $Ra=10^4$ .


 FIG. 16. Isothermal lines at  $Ra=10^5$ .

measured at temperature  $T_c$ ,  $H$  is the height of the cavity, and  $g$  is the gravity acceleration.

We carried out our simulations on a  $128 \times 128$  mesh for  $Pr=0.71$  with  $Ra$  varying from  $10^3$  to  $10^5$ . The nondimensional temperature difference  $(T_h - T_c)/T_c$  is set to be within 5%. It is noted that the present MRT-LBE model is a coupling model and the Boussinesq approximation is not necessary.

The streamlines and isothermal lines predicted by the present model are shown in Figs. 11–16. From the figures, it is shown that for low values of  $Ra$ , a central vortex appears as the typical features of the flow. The vortex tends to become elliptic as  $Ra$  increases, and breaks up into two vortices at  $Ra=10^5$ . All of these observations are in good agreement with the results reported in previous studies [20,44]. For a quantitative comparison, the average Nusselt numbers are measured and listed in Table I. The numerical results are in quantitative agreement with those reported in previous studies [20,44], but some small differences in the average Nusselt numbers are also noticed, which may be the effects of the viscous dissipation and the work of the pressure in our model.

The normalized velocity profiles  $u_x$  ( $u_y$ ) in Fig. 17 (Fig. 18) recovered with the TMRT model along the vertical (horizontal) lines, and in Fig. 19 the temperature profiles along the horizontal line crossing the center of the cavity are also compared with the numerical results in the literature [45]. As shown in Figs. 17 and 18, the maximum value of  $u_x(u_y)$  along the vertical (horizontal) lines increases as  $Ra$  becomes large. Figure 19 indicates that the heat transfers mainly by conduction between the hot and cold walls for small  $Ra$ . When  $Ra$  becomes large, the dominant heat transfer mechanism changes from conduction to convection, and the heat transfer becomes large at the thin boundary layers near the

TABLE I. The average Nusselt number.

Ra	Nu		
	Present	Reference [20]	Reference [44]
$10^3$	1.174	1.119	1.116
$10^4$	2.266	2.254	2.244
$10^5$	4.528	4.527	4.521

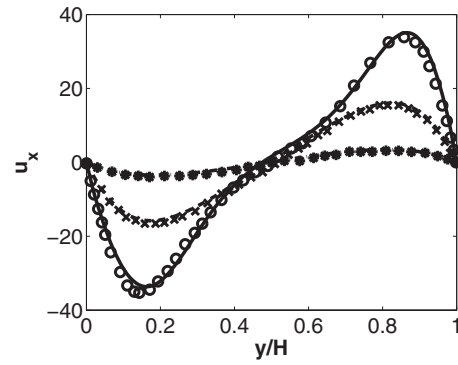


FIG. 17. Normalized velocity profile for  $u_x$  along the center line of the cavity in the  $y$  direction. Symbols are from Ref. [45], lines are the LBE results. Asterisk and dashed-dotted line,  $Ra=10^3$ ; cross and dashed line,  $Ra=10^4$ ; open circle and solid line,  $Ra=10^5$ .

hot and cold walls. It is also clearly seen from Figs. 17–19 that the numerical results of the present LBE model agree well with those reported in Ref. [45].

## V. CONCLUSION

In this paper, we have developed a LBE model with multiple relaxation times for thermal flows. The model exhibits several features that distinguish it from other previous LBE models. First, unlike previous thermal LBE models, the present model does not suffer from the fixed Prandtl number problem due to the use of multiple relaxation times; second, the inconsistency existing in the viscous terms in the momentum and energy equations is also successfully overcome by modifying the collision processes of the moments related to the energy flux; finally, the energy momentum equations derived from the present model are physically coupled, which makes it feasible for non-Boussinesq flows.

Some numerical simulations have been carried out to validate the proposed MRT LBE model. It is found that the results predicted by the present TMRT model are in excellent agreement with the analytical solutions and/or other numerical results.

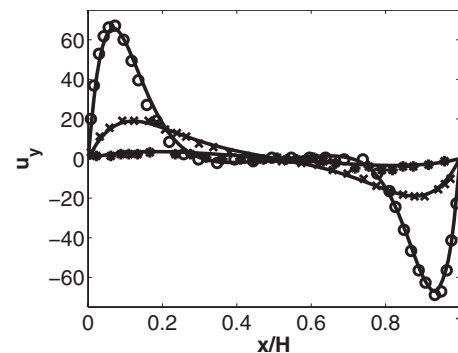


FIG. 18. Same as Fig. 17 but for the normalized velocity profile for  $u_y$  along the center line of the cavity in the  $x$  direction.

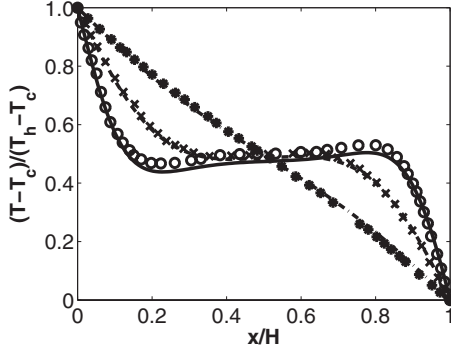


FIG. 19. Same as Fig. 17 but for the temperature profile along the center line of the cavity in the  $x$  direction.

### ACKNOWLEDGMENTS

The authors would like to thank Dr. H. F. Han and Dr. Z. H. Chai for helpful discussions. This work is supported by the National Natural Science Foundation of China (Contracts No. 50606012 and No. 60773195) and the National Basic Research Program of China (Contract No. 2006CB705804).

### APPENDIX: CHAPMAN-ENSKOG ANALYSIS FOR THERMAL MULTIPLE-RELAXATION-TIME MODEL

We now make an analysis for the TMRT model using the Chapman-Enskog expansion method [46]. To this end, we introduce the following expansions:

$$f_i = \sum_{n \geq 0} K^n f_i^{(n)}, \quad (\text{A1})$$

$$\partial_t = \sum_{n \geq 0} K^n \partial_{t_n}, \quad (\text{A2})$$

$$f_i(\mathbf{x} + \mathbf{c}_i \delta t, t + \delta t) = \sum_{n \geq 0} K^n \frac{(\partial_t + \mathbf{c}_i \cdot \nabla)^n}{n!} f_i(\mathbf{x}, t), \quad (\text{A3})$$

where  $K$  is the expansion parameter, which is equal to  $\delta t$ .

Through the above expansions, we can obtain the following relationship for Eq. (1) with the zeroth-, first-, and second-order expansions in  $K$ :

$$f_i^{(0)} = f_i^{(eq)}, \quad (\text{A4})$$

$$(\partial_{t_0} + \mathbf{c}_i \cdot \nabla) f_i^{(0)} = - \sum_{\alpha} \mathbf{S}_{i\alpha} f_{\alpha}^{(1)} + F_i, \quad (\text{A5})$$

$$\partial_{t_1} f_i^{(0)} + (\partial_{t_0} + \mathbf{c}_i \cdot \nabla) \left[ \sum_{\beta} \left( \mathbf{I}_{i\beta} - \frac{\mathbf{S}_{i\beta}}{2} \right) f_{\beta}^{(1)} \right] = - \sum_{\alpha} \mathbf{S}_{i\alpha} f_{\alpha}^{(2)}. \quad (\text{A6})$$

The corresponding equations in the moment space can be obtained

$$m_i^{(0)} = m_i^{(eq)}, \quad (\text{A7})$$

$$(\partial_{t_0} + \tilde{\mathbf{c}}_i \partial_i) \mathbf{m}^{(0)} = \tilde{\mathbf{S}} \mathbf{m}^{(1)} + \tilde{\mathbf{F}}, \quad (\text{A8})$$

$$\partial_{t_1} \mathbf{m}^{(0)} + (\partial_{t_0} + \tilde{\mathbf{c}}_i \partial_i) \left( \mathbf{I} - \frac{\tilde{\mathbf{S}}}{2} \right) \mathbf{m}^{(1)} = - \tilde{\mathbf{S}} \mathbf{m}^{(2)}, \quad (\text{A9})$$

where  $\tilde{\mathbf{c}}_i = \mathbf{M}(\mathbf{c}_{i\alpha} \mathbf{I}) \mathbf{M}^{-1}$  and

$$\mathbf{m}^{(1)} = [0, 0, 0, 0, p_{xx}^{(1)}, p_{xy}^{(1)}, \varepsilon^{(1)}, \pi_{xx}^{(1)}, \pi_{xy}^{(1)}, h^{(1)}, H^{(1)}, q_x^{(1)}, \eta_x^{(1)}, \gamma_x^{(1)}, q_y^{(1)}, \eta_y^{(1)}, \gamma_y^{(1)}]^T. \quad (\text{A10})$$

The first four equations for the conserved moments can be written as

$$\partial_{t_0} \rho + \partial_x(\rho u_x) + \partial_y(\rho u_y) = 0, \quad (\text{A11})$$

$$\partial_{t_0}(\rho u_x) + \partial_x(\rho \varepsilon + \rho u_x^2) + \partial_y(\rho u_x u_y) = \rho a_x, \quad (\text{A12})$$

$$\partial_{t_0}(\rho u_y) + \partial_x(\rho u_x u_y) + \partial_y(\rho \varepsilon + \rho u_y^2) = \rho a_y, \quad (\text{A13})$$

$$\partial_{t_0}(\rho E) + \partial_x[(\rho \varepsilon + \rho E) u_x] + \partial_y[(\rho \varepsilon + \rho E) u_y] = \rho(u_x a_x + u_y a_y), \quad (\text{A14})$$

$$\partial_{t_1} \rho = 0, \quad (\text{A15})$$

$$\partial_{t_1}(\rho u_x) + \partial_x \left[ \frac{1}{2} \left( 1 - \frac{s_4}{2} \right) p_{xx}^{(1)} \right] + \partial_y \left[ \left( 1 - \frac{s_5}{2} \right) p_{xy}^{(1)} \right] = 0, \quad (\text{A16})$$

$$\partial_{t_1}(\rho u_y) + \partial_x \left[ \left( 1 - \frac{s_5}{2} \right) p_{xy}^{(1)} \right] + \partial_y \left[ \frac{1}{2} \left( 1 - \frac{s_4}{2} \right) p_{xx}^{(1)} \right] = 0, \quad (\text{A17})$$

$$\partial_{t_1}(\rho E) + \partial_x \left[ \frac{1}{6} \left( 1 - \frac{s_{11}}{2} \right) q_x^{(1)} \right] + \partial_y \left[ \frac{1}{6} \left( 1 - \frac{s_{14}}{2} \right) q_y^{(1)} \right] = 0. \quad (\text{A18})$$

Meanwhile,

$$\begin{aligned} -s_4 p_{xx}^{(1)} &= \partial_{t_0} p_{xx}^{(eq)} + \frac{17}{15} [\partial_x(\rho u_x) - \partial_y(\rho u_y)] \\ &\quad - \frac{47}{465} (\partial_x q_x^{(eq)} - \partial_y q_y^{(eq)}) - \frac{4}{5} (\partial_x \eta_x^{(eq)} - \partial_y \eta_y^{(eq)}) \\ &\quad + \frac{8}{155} (\partial_x \gamma_x^{(eq)} + \partial_y \gamma_y^{(eq)}) - 2\rho(u_x a_x - u_y a_y), \end{aligned} \quad (\text{A19})$$

$$\begin{aligned} -s_5 p_{xy}^{(1)} &= \partial_{t_0} p_{xy}^{(eq)} + \frac{34}{15} [\partial_x(\rho u_y) + \partial_y(\rho u_x)] \\ &\quad + \frac{101}{465} (\partial_x q_y^{(eq)} + \partial_y q_x^{(eq)}) + \frac{2}{5} (\partial_x \eta_y^{(eq)} + \partial_y \eta_x^{(eq)}) \\ &\quad + \frac{4}{155} (\partial_x \gamma_y^{(eq)} - \partial_y \gamma_x^{(eq)}) - \rho(u_x a_y + u_y a_x), \end{aligned} \quad (\text{A20})$$

$$\begin{aligned} -s_{11} q_x^{(1)} &= \partial_{t_0} q_x^{(eq)} + \frac{31}{109} \partial_x E' - \frac{47}{17} \partial_x p_{xx}^{(eq)} \\ &\quad + \frac{101}{17} \partial_y p_{xy}^{(eq)} + \frac{3}{109} \partial_x \varepsilon^{(eq)} + \frac{18}{17} \partial_x \pi_{xx}^{(eq)} + \frac{72}{17} \partial_y \pi_{xy}^{(eq)} \\ &\quad + \{17\rho a_x - 6[\rho u_x(u_x a_x + u_y a_y) + \rho \varepsilon a_x + \rho E a_x]\}, \end{aligned} \quad (\text{A21})$$

$$\begin{aligned}
 -s_{14}q_y^{(1)} &= \partial_{t_0}q_y^{(eq)} + \frac{31}{109}\partial_y E' - \frac{47}{17}\partial_y p_{xx}^{(eq)} \\
 &+ \frac{101}{17}\partial_x p_{xy}^{(eq)} + \frac{3}{109}\partial_y \varepsilon^{(eq)} + \frac{18}{17}\partial_y \pi_{xx}^{(eq)} + \frac{72}{17}\partial_x \pi_{xy}^{(eq)} \\
 &+ \{17\rho a_y - 6[\rho u_y(u_x a_x + u_y a_y) + \rho \varepsilon a_y + \rho E a_y]\}.
 \end{aligned} \tag{A22}$$

With the aid of Eqs. (A11)–(A14) and the equilibria of the nonconserved moments, we could obtain  $p_{xx}^{(1)}$ ,  $p_{xy}^{(1)}$ ,  $q_x^{(1)}$ , and  $q_y^{(1)}$  in Eqs. (A16)–(A18) as follows:

$$p_{xx}^{(1)} = -\frac{2}{s_4}\rho\epsilon(\partial_x u_x - \partial_y u_y), \tag{A23}$$

$$p_{xy}^{(1)} = -\frac{1}{s_5}\rho\epsilon(\partial_x u_y + \partial_y u_x), \tag{A24}$$

$$q_x^{(1)} = -\frac{6}{s_{11}}\left(2\rho\epsilon\partial_x \epsilon - \frac{s_4}{2}u_x p_{xx}^{(1)} - s_5 u_y p_{xy}^{(1)}\right), \tag{A25}$$

$$q_y^{(1)} = -\frac{6}{s_{14}}\left(2\rho\epsilon\partial_y \epsilon + \frac{s_5}{2}u_y p_{xx}^{(1)} - s_5 u_x p_{xy}^{(1)}\right). \tag{A26}$$

Combining Eqs. (A11)–(A18), we are able to obtain the thermohydrodynamic equations (25)–(27) with  $s_4=s_5$  and  $s_{11}=s_{14}$ . Finally, with the modified collision process, the correct thermohydrodynamic equations are recovered by Eqs. (31) and (32).

- 
- [1] R. Benzi, S. Succi, and M. Vergassola, *Phys. Rep.* **222**, 145 (1992).
  - [2] S. Chen and G. Doolen, *Annu. Rev. Fluid Mech.* **30**, 329 (1998).
  - [3] G. R. McNamara and G. Zanetti, *Phys. Rev. Lett.* **61**, 2332 (1988).
  - [4] Y. Chen, H. Ohashi, and M. Akiyama, *Phys. Rev. E* **50**, 2776 (1994).
  - [5] F. J. Alexander, S. Chen, and J. D. Sterling, *Phys. Rev. E* **47**, R2249 (1993).
  - [6] Y. Qian, *J. Sci. Comput.* **68**, 231 (1993).
  - [7] M. Watari and M. Tsutahara, *Physica A* **382**, 502 (2007).
  - [8] B. Piaud *et al.*, *J. Stat. Phys.* **121**, 119 (2005).
  - [9] P. C. Philippi, L. A. Hegele, Jr., L. O. E. dos Santos, and R. Surmas, *Phys. Rev. E* **73**, 056702 (2006).
  - [10] N. I. Prasianakis and I. V. Karlin, *Phys. Rev. E* **76**, 016702 (2007).
  - [11] V. Sofonea, *Phys. Rev. E* **74**, 056705 (2006).
  - [12] V. Sofonea, *Europhys. Lett.* **76**, 829 (2006).
  - [13] G. Gonnella, A. Lamura, and V. Sofonea, *Phys. Rev. E* **76**, 036703 (2007).
  - [14] Y. Gan *et al.*, *Physica A* **387**, 1721 (2007).
  - [15] X. Pan *et al.*, *Int. J. Mod. Phys. C* **18**, 1747 (2007).
  - [16] X. Shan, *Phys. Rev. E* **55**, 2780 (1997).
  - [17] Z. L. Guo, B. C. Shi, and C. G. Zheng, *Int. J. Numer. Methods Fluids* **39**, 325 (2002).
  - [18] X. He, S. Chen, and G. D. Doolen, *J. Comput. Phys.* **146**, 282 (1998).
  - [19] Y. Shi, T. S. Zhao, and Z. L. Guo, *Phys. Rev. E* **70**, 066310 (2004).
  - [20] Z. L. Guo, C. G. Zheng, B. C. Shi, and T. S. Zhao, *Phys. Rev. E* **75**, 036704 (2007).
  - [21] Y. Peng, C. Shu, and Y. T. Chew, *Phys. Rev. E* **68**, 026701 (2003).
  - [22] A. D’Orazio, S. Succi, and C. Arrighetti, *Phys. Fluids* **15**, 2778 (2003).
  - [23] A. D’Orazio and S. Succi, *FGCS, Future Gener. Comput. Syst.* **20**, 935 (2004).
  - [24] A. D’Orazio and S. Succi, *Lect. Notes Comput. Sci.* **2657**, 977 (2003).
  - [25] P. Lallemand and L.-S. Luo, *Phys. Rev. E* **68**, 036706 (2003).
  - [26] X. Shan, X. F. Yuan, and H. Chen, *J. Fluid Mech.* **550**, 413 (2006).
  - [27] X. B. Nie, X. Shan, and H. Chen, *Europhys. Lett.* **81**, 34005 (2008).
  - [28] G. R. McNamara, A. L. Garcia, and B. J. Alder, *J. Stat. Phys.* **87**, 1111 (1997).
  - [29] Y. Chen, H. Ohashi, and M. Akiyama, *J. Sci. Comput.* **12**, 169 (1997).
  - [30] H. Chen, C. Teixeira, and K. Molving, *Int. J. Mod. Phys. C* **8**, 675 (1997).
  - [31] M. Soe, G. Vahala, P. Pavlo, L. Vahala, and H. Chen, *Phys. Rev. E* **57**, 4227 (1998).
  - [32] P. L. Bhatnagar, E. P. Gross, and M. Krook, *Phys. Rev.* **94**, 511 (1954).
  - [33] D. d’Humières, in *Progress in Astronautics and Aeronautics*, edited by B. D. Shizgal and D. P. Weaver (AIAA, Washington, DC, 1992), Vol. 159, p. 450.
  - [34] P. Lallemand and L.-S. Luo, *Phys. Rev. E* **61**, 6546 (2000).
  - [35] D. d’Humières, M. Bouzidi, and P. Lallemand, *Phys. Rev. E* **63**, 066702 (2001).
  - [36] M. E. McCracken and J. Abraham, *Phys. Rev. E* **71**, 036701 (2005).
  - [37] X. Shan and H. Chen, *Int. J. Mod. Phys. C* **18**, 635 (2007).
  - [38] Z. L. Guo, C. G. Zheng, and B. C. Shi, *Phys. Rev. E* **65**, 046308 (2002).
  - [39] M. A. Gallivan, D. R. Noble, J. G. Georgiads, and R. O. Buckius, *Int. J. Numer. Methods Fluids* **25**, 249 (1997).
  - [40] Q. Zou and X. He, *Phys. Fluids* **9**, 1591 (1997).
  - [41] R. S. Maier and R. S. Bernard, *Int. J. Mod. Phys. C* **8**, 747 (1997).
  - [42] Z. L. Guo, C. G. Zheng, and B. C. Shi, *Phys. Fluids* **14**, 2007 (2002).
  - [43] V. Sofonea and R. F. Sekerka, *Phys. Rev. E* **71**, 066709 (2005).
  - [44] M. Hortmann and M. Perić, *Int. J. Numer. Methods Fluids* **11**, 189 (1990).
  - [45] A. D’Orazio, M. Corcione, and G. P. Celata, *Int. J. Therm. Sci.* **43**, 575 (2004).
  - [46] S. Chapman and T. G. Cowling, *The Mathematical Theory of Non-Uniform Gases*, 3rd ed. (Cambridge University Press, Cambridge, UK, 1970).